JLAB USER GROUP

Jefferson Lab PAC18
Proposal Cover Sheet

This document must be received by close of business Thursday,

June 1, 2000 at:

Jefferson Lab
User Liaison,
Mail Stop 12B
12000 Jefferson Ave.
Newport News, VA
23606

Experimental Hall: C

Days Requested for Approval: 30

❒ **Proposal Title:**
Auger Neutron Spectroscopy of Nuclear Matter at CEBAF

Proposal Physics Goals
Indicate any experiments that have physics goals similar to those in your proposal.

Approved, Conditionally Approved, and/or Deferred Experiment(s) or proposals:

Contact Person

Name: A. Margaryan
Institution: Yerevan Physics Institute
Address: 2 Alikhanian Bros. st.
Address:
City, State, ZIP/Country: Yerevan - 36, 375036, Armenia
Phone: 3742350030 **Fax:** 3742350030
E-Mail: amour@jlab.org; mat@jerewan1.yerphi.am

Jefferson Lab Use Only

Receipt Date: 5/11/00

By: [redacted]

LOI 00-101

Auger Neutron Spectroscopy of Nuclear Matter at CEBAF

Jlab PAC 18 Letter of Intent

A. Margaryan (contact person)
Yerevan Physics Institute, 2 Alikhanian Bros. St.,
Yerevan-36, 375036, Armenia

L. Tang
H*ampton University, Hampton, VA 23668, USA*

S. Majewski
JLAB, 12000 Jefferson Avenue, Newport News, VA 23606, USA

O. Hashimoto
Tohoku University, Sendai, 980-8578, Tohoku, Japan

V. Likhachev
Institute Fisica, USP, Rua do Matao, trav. 187, CEP-05508-900,
Sao Paulo, Brazil

Abstract

We propose to perform precise spectroscopy of heavy hypernuclei using the nuclear Auger effect. Auger neutron spectroscopy of heavy hypernuclei (Pb, U) is the most direct way to study the shell structure of strongly bound Λ particles in the 1s, 1d, 1f, 2p, 1g, 2d, and 1h orbits. This measurement is a stringent test of the nuclear shell structure for deeply bound states. A heavy hypernuclear spectrometric measurement must have a relative precision better than 50 keV. The absolute value of the 1d-1s transition energy will be determined with a precision of a few keV.

These investigations will fully utilize the unique parameters of the CEBAF electron beam and RF system, and are enabled by (1) the use of neutron timing detectors based on the recently developed low-pressure MWPCs and (2) the development of an RF timing technique for fission fragments with picosecond resolution.

The RF timing technique will enable to tag up to 1000 heavy hypernuclei per second at CEBAF. This can be used for a detailed study of the four-baryon weak interaction.

1. Introduction

One of the open questions of nuclear physics is how literally we can extrapolate the shell structure to strongly bound levels [1]. The nuclear hole states produced in heavy nuclei are so broad that no quantitative information on their binding energies and even less on their wave functions can be obtained. Much effort has been put into electron scattering experiments [2,3] to find out whether the charge distribution of the 3s state in the lead region corresponds to the shell model prediction. The 3s proton is just barely bound but its probability distribution is peaked at zero radius. The proton wave function seems to be quite well described even at small distances by the shell model and has an overall overlap of about 65% with the shell model wave function. There is no direct experimental evidence that in heavy nuclei like lead a classification of the nucleons 1s, 1p, 1d, 2s shells is justified.

On the other hand, the Λ-particle bound to a nucleus is an excellent probe of nuclear properties; it has mass M_Λ = 1115 MeV, exceeding the mass of a nucleon by less than 20%. The Λ-nucleus interaction is only slightly weaker than the N-nucleus one. Therefore, we can expect the Λ-particle in the nucleus to behave very much like a neutron - a neutron, however, with the strangeness quantum S=-1 that can be distinguished from other nucleons.

The Λ single particle states in heavy hypernuclei, as has been shown theoretically, are much narrower than their spacing and, therefore, suitable for spectroscopy [4]. Fig. 1 shows an excitation spectrum in $^{89}{}_{\Lambda}$Y obtained at the Brookhaven AGS, showing s, p, d, f, and g Λ-orbitals [5]; it demonstrates in a striking way the validity of the concept of shell model orbitals, not just in the valence region, but deep within the nuclear interior. The spectrum of Fig.1 was taken with a resolution of 2.6 MeV FWHM, and only the major shell orbitals are resolved. Precise determination of the Λ level spacing can help to more stringently test the standard mean field picture, such as partial deconfinement of the strange quark in the Λ inside the nucleus. The spin-dependent components of the ΛN interaction are small. One needs an energy resolution of several hundred keV to measure the fine structure of the peaks. A detailed shell model calculation of the hypernuclear excited states has been performed for the ^{208}Pb nucleus [6]. It was shown that the widths of the levels do not depend strongly on the choice of the potential parameters for the Λ-particle in the lead nucleus, and for deeply bound states are of the order of 100 keV or less. A properly designed experiment with high energy resolution has a good chance to follow the Λ-particle down the excitation ladder to the 1s state. However, in the traditional way by missing mass measuring, one can reach an energy resolution of about one MeV [7].

For the Λ-particle in a highly excited state the most important mechanism of deexcitation is the nuclear Auger effect [6]. Due to this effect the Λ hyperon jumps from higher to lower shell states emitting monochromatic neutrons because its lifetime, $\tau \approx 10^{-10}$, is long enough that its weak decay $\Lambda N \rightarrow NN$ takes place in the 1s ground state (Fig.2). The

protons can be ignored because of the Coulomb barrier. The probability for the Auger emission is many orders of magnitude larger than for the gamma emission, except for the 1p-1s transition for which neutron emission is forbidden energetically.

Because kaon photoproduction is the weakest nuclear interaction involving a hadron it is the ideal reaction for the excitation of Λ hypernuclear states. Medium and high spin states are preferentially excited [8]. These excited states will emit monochromatic Auger neutrons in the 1-10 MeV range, and the Λ will settle at the 1s state before decaying weakly.

We propose to measure the energies of these monochromatic neutrons at CEBAF. The proposed technique provides effective, up to 90%, tagging of the produced heavy hypernuclei and better than 50 keV energy resolution for 1 MeV neutrons. This is new spectroscopy of nuclear matter, allowing the investigation of the inner shell structure of heavy nuclei with high precision, and it is the most precise heavy hypernuclear spectroscopy which can be done in the near future.

2. Nuclear Auger Effect

Substitution states in heavy hypernuclei have an excitation of about 25 MeV. The Λ threshold in heavy hypernuclei is much higher (~ 28 MeV) than the nucleon one (~ 8 MeV). Thus the excited states will decay due to the nuclear Auger effect with emission of neutrons (Fig. 2). The protons can be ignored because of the Coulomb barrier. The Auger effect describes the following process [6]:

$$\Lambda(n_1 l_1 m_1 s_1) + n(n_2 l_2 j_2 m_2) \rightarrow \Lambda(n_3 l_3 m_3 s_3) + n(k l_4 j_4 m_4)$$

where n_1 and n_3 denote the main quantum numbers of the bound Λ, and n_2 of the bound neutron and l, j, m, and μ are the angular momentum quantum numbers. The outgoing neutron is characterized by $n(kl_4j_4\mu_4)$ where k is the particle momentum.

The partial transition probability for the nuclear Auger effect in the channel β is given by

$$\hbar w_b = \frac{4}{\hbar V_b} \frac{1}{2(2l_1+1)} \sum \left| \int d^3 r_n d^3 r_\Lambda \psi_4(r_n) \psi_3(r_\Lambda) V(r_{n\Lambda}) \psi_2(r_n) \psi_1(r_\Lambda) \right|^2$$

where the summation is performed over all magnetic quantum numbers. The velocity V_β = hk/m is the velocity of the outgoing neutron in the channel β. The total transition probability is:

$$\hbar w = \sum_b \hbar w_b$$

The reduction of the transition probability for Λ particles has been realized by the following considerations. The residual interaction $V_{\Lambda N}$ is in general weaker than the V_{NN}. The Λ-particle jumps from higher to lower shell-model states, calculated with Woods-Saxon potential. There is no spin-orbit force for Λ.

1. One neutron is ejected from a lower state into the continuum. The first order perturbation formula is used for the process $\Lambda + n \rightarrow \Lambda' + n'$.

2. The initial neutron state is assumed to have a sharp energy. The final neutron state (in the continuum) also feels an imaginary optical potential.

3. The protons are ignored because of the Coulomb barrier.

4. The spin dependent part of $V_{\Lambda N}$ is very weak and the spin-vector modes are very weakly excited.

The single-particle wave functions of Λ and neutron correspond to the Woods-Saxon potential of the form

$$V = -V_c f_c(r) + \left(\frac{h}{m_p c} \right)^2 V_{so} \boldsymbol{s} \cdot \boldsymbol{l} * \frac{1}{r} \frac{d f_{so}(r)}{dr} + 4iV_i a_i \frac{d f_i(r)}{dr}$$

where

$$f_a(r) = 1/\left(1 + \exp\left(\left(r - r_a\right)/a_a\right)\right)$$

As an example for heavy hypernuclei, $^{208}_{\Lambda}$Pb has been chosen arbitrarily. Two choices for the potential were made in order to see how sensitive the results are ("the theoretical error bar"). The parameters used in this calculation are given in Table 1. Choice B (broader and shallower V) is adapted to have the same width as the nucleon potential, while choice A (narrower and deeper) seems to have a more standard depth.

Table 1. The parameters of the Woods-Saxon potential

α	V_α	$R_\alpha A^{-1/3}$	A_α	
c	49.3 MeV -0.33 E	1.25 fm	0.65 fm	for outgoing neutron
SO	5.5	1.25	0.65	
i	5.75	1.25	0.70	
c	44.137	1.27	0.67	For bound neutron
SO	7.68	1.27	0.67	
i	0			
c	32.5	1.1	0.60	For Λ (choice A)
SO	0			
i	0			
c	22.8	1.27	0.67	For Λ (choice B)
SO	0			
i	0			

Table 2 shows the Λ single particle energies and transition rates obtained with both sets of parameters. The first and second column give the Auger transition rates summed over all final states β for two choices of the Λ wave functions. The potential of the outgoing neutron (Table 1) includes also a small imaginary part. Therefore, the presented Auger rates correspond to the neutron escape process which we are interested in. The third and forth column give gamma transition rates. They are typically 1000 times less probable than the Auger transitions for all the states except the lowest two. Whereas the 1p Λ state with an excitation energy of 3 MeV can decay only via gamma transition, there is a very sensitive energy balance for the 1d state which determines whether the Auger effect is possible or not.

Table 2. The single particle energies, the Auger (h? $_0$) and gamma (h? $_g$) transition rates of the Λ particle in ^{208}Pb.

Initial state	E_Λ (MeV) Choice A	E_Λ (MeV) Choice B	h? $_0$ (keV) Choice A	h? $_0$ (keV) Choice B	h? $_\gamma$ (keV) Choice A	h? $_\gamma$ (keV) Choice B
1i	+6.0	+6.0	306	51	0.2082	0.1728
2f	+1.0	+1.0	396	58		
1h	-1.154	-0.108	167	22	0.1372	0.0744
3s	-4.275	-2.451	446	128		
2d	-5.019	-2.961	334	69		
1g	-7.639	-4.885	91	14	0.0968	0.0528
2p	-11.345	-7.602	262	37		
1f	-13.737	-9.387	47	2	0.0601	0.0327
2s	-17.608	-12.228	109	23		
1d	-19.293	-13.489	10	0	0.0309	0.0168
1p	-24.183	-17.095	0	0	0.0108	0.0058
1s	-28.275	-20.106				

For the calculated Λ spectrum and assuming that the 1d state is populated directly with emitting one Auger neutron from $^{208}_{\Lambda}$Pb, the excitation energy of the 1d Λ-particle (7 MeV) is smaller than the separation of the last neutron in ^{206}Pb, which is 8.09 MeV. Therefore it will depend on the particular choice of the hypernucleus whether the 1d Λ-state of $^{207}_{\Lambda}$Pb hypernucleus will decay via gamma or Auger transition.

Population of the Λ states after one or two neutrons are emitted from $^{208}_{\Lambda}$Pb is given in Table 3 for both choices of parameters.

Table 3. Population of L states after one ore two Auger neutrons are emitted from $^{208}_{L}$Pb

Potential	Choice A		Choice A		Choice B		Choice B	
Initial Λ state	1i		1h		1I		1h	
Auger neutrons	1	2	1	2	1	2	1	2
3s	0.001				0.000			
2d	0.022				0.005			
1g	0.113				0.125			
2p	0.036		0.008		0.037		0.001	
1f	0.266	0.000	0.175		0.318		0.043	
2s	0.030	0.004	0.037		0.040	0.000	0.064	
1d	0.295	0.039	0.400	0.000	0.267	0.025	0.543	
1p	0.189	0.266	0.292	0.126	0.166	0.177	0.243	0.012
1s	0.048	0.453	0.088	0.495	0.041	0.324	0.106	0.096

Energy spectra of the Auger neutrons after the deexcitation of 1h state of $^{208}_{\Lambda}$Pb for A and B choices of the Λ potential are displayed in Fig.3[a,b]. The energy distributions of the Auger neutrons have been obtained via a Monte Carlo simulation, taking into account the energies and widths of the Λ levels, partial transition rates, and the separation energies of neutrons ^{207}Pb and ^{206}Pb (6.7 and 8.09 MeV respectively). It is interesting to note that the emission of one Auger neutron leads to the population of the 1p and 1d states of $^{207}_{\Lambda}$Pb in as many as 50% of all cases. Finally, the 1d-1s transition results in monochromatic neutrons with energies 1-2 MeV. What is extremely important is that the widths of the levels are essentially smaller than the separation of the major Λ shells for both choices of the potential parameters. In conclusion, we can state that Auger neutron spectroscopy is accessible to experiments if a suitable way to produce and detect Auger neutrons and measure their energies with sufficiently good resolution can be found.

3. Hypernuclear Excitation through Kaon Photoproduction

Because kaon photoproduction is the weakest nuclear interaction involving a hadron it is the ideal reaction for the excitation of Λ hypernuclear states. The reaction mechanism is reasonably well understood and is amenable to an accurate theoretical description. In the plane wave impulse approximation, multiple-scattering calculations for hypernuclear formation from a ^{208}Pb target were performed by Hsiao and Cotanch [8] for a wide range of lab and excitation energies. Excitation energies and transition densities were calculated using Woods-Saxon basis wave functions. The transition operator was constructed using the free amplitudes for the elementary process $p(\gamma, K^+)\Lambda$ which are evaluated from Feynman diagrams including both strange meson (K, K*) and baryon (Λ,Σ) exchange. The selective excitation of hypernuclei is documented in detail for θ = 0°. Because of the large momentum transfer ($\geq$ 200 MeV/c), the (γ, K) reaction is highly quasielastic, and the Λ "sticking probability" is about 0.1. The distribution of strength for the substitutional states ($p\rightarrow\Lambda$ in the same orbital configuration) is illustrated in Fig.5, for the reaction ^{208}Pb(γ, K^+) $^{208}_{\Lambda}$Tl at energies 1.2 GeV (dashed lines) and 2.0 GeV (solid lines). One can see that medium and high spin states such as the 1p, 1d, 1f, 1g, and 1h states are preferentially excited. Among them the most pronounced state is the 1d state. The electromagnetic production of the Λ hypernuclei can be considered also for the reaction $n(\gamma, K^0)\Lambda$ [9]. The cross section and kinematics of this reaction are practically the same as for (γ, K^+) reaction. Therefore, the reaction ^{208}Pb(γ, K^0) $^{208}_{\Lambda}$Pb will populate Λ states in ^{208}Pb practically with the same probability as we have for ^{208}Tl.

From the calculations presented in [6] it follows that the probability for the Auger emission is many orders of magnitude larger than for gamma emission, and that these excited states will emit monochromatic Auger neutrons, and Λ will settle at the 1s-state before its weak decay (Fig.3). The emission of one Auger neutron from higher excited states also leads to the population of the 1p and 1d states. Due to these deexcitation processes about 1-2 Auger neutrons will be produced in the energy range 1-10 MeV. The neutral width of these states, which is determined mainly by the probability of the Auger emission, is about or less than 100 keV, and the typical level spacing is about 2 MeV. The spin dependent components of the ΛN interaction is expected to be an order of magnitude smaller. Therefore, a resolution of the order of few hundred keV is likely to be necessary for the Auger neutron spectroscopy.

The exception is the 1p-1s transition and maybe, in special cases, the cascade 1d $\rightarrow$ 1p $\rightarrow$ 1s (see Table 2), where Auger emission is forbidden energetically. Then the electromagnetic transition takes over. Therefore, γ-spectroscopy is of interest only if the transitions between the $1p\rightarrow1s$ Λ major shells in heavy hypernuclei are investigated or if the nuclear core excitations with a Λ particle in the 1s state are studied.

4. Auger Neutron Spectroscopy at CEBAF

We propose to use the electron beam in Hall C at TJNAF to carry out Auger neutron spectroscopy in the energy range 1-10 MeV via photoproduction of excited Λ-states in heavy nuclei. A great number of neutrons are generated when an electron beam hits a target. According to a simulation with a Monte Carlo code [10], the cross

section for the production of background neutrons with energies lower than 10 MeV in a 1.6 GeV electron and for a lead target is: $\sigma(e+Pb \rightarrow n+X) \approx 30$ mb. The expected cross section of the production of heavy hypernuclei is about 5 orders of magnitude smaller. Therefore, for Auger neutron spectroscopy one needs to detect and measure the energies of monochromatic neutrons produced by the nuclear Auger effect in a huge amount of background neutrons. We propose to carry out precise measurements of the energies of these monochromatic Auger neutrons using the time-of-flight technique.

The primary experimental equipment (see Fig. 5) required in the proposed experiment includes (1) the Hall C electron beam and RF source, (2) the RF picosecond timing technique for fission fragments, (3) timing neutron detectors based on low-pressure MWPCs and (4) the Short Orbit Spectrometer(SOS) in Hall C.

4.1 Electron Beam and RF Source

We plan to use a 2 GeV CW electron beam with up to 100 μA in Hall C to produce enough heavy hypernuclei for Auger neutron spectroscopy. We need an RF source, from the appropriate accelerator RF circuit, to feed the resonators for the RF timing technique.

4.2 The RF Picosecond Timing Technique for Fission Fragments

The RF picosecond timing technique for fission fragments [11,12] will be used for the detection and separation of the delayed fission events associated with heavy hypernuclei. It will be used also for the determination of the number of the bucket in which the hypernucleus is produced. Therefore, the production time of heavy hypernuclei (Auger neutrons) will be determined within 1.67 ps precision. The properties of this technique- picosecond time resolution, high efficiency (~90%) for the unambiguous detection of delayed fission fragments, and insensitivity to gamma and relativistic particles- make Auger neutron spectroscopy possible at CEBAF.

The idea of using RF fields to achieve picosecond timing has received considerable attention in the past. For instance, a resonant microwave cavity was used previously as a deflecting system to investigate the structure of electron bunches in a linear accelerator [13] and a microtron [14]. In these papers, a 2 ps time resolution had been reported. In a photocathode RF electron gun, 0.5 ps time resolutions have been recently reached [15].

Johanson and Alvager [16] suggested to use this method for measuring short nuclear half-lives in the picosecond and sub-picosecond range. Nuclear lifetimes in the range 10-100 ps have been measured with the help of these techniques [17-22].

.

Recently it had been proposed to use the principles of a picosecond time resolution to identify and measure delayed fragments at CEBAF based on the RF analysis of secondary electrons emitted from a target [11]. Electron/photon beams interacting with a surface of matter produce secondary electrons. Other charged particles passing through the target surface also produce secondary electrons in proportion with their energy loss in matter. The characteristic energies of these electrons are about 2 eV, and they are emitted from a thickness on the order of 10^{-5} cm, and the

time scale of the process is less than 0.1 ps. The inherent time dispersion of the secondary emission process was measured to be about 4 ps or less [23]. Therefore secondary electrons originate with the same time structure as that of the incident beam or secondary particles (1.67 ps width each 2 ns interval at CEBAF experimental halls), and that has long been used for time measurements in experimental nuclear physics [24-26]. The time scale for the secondary electrons from decay processes (e.g., delayed fission associated with Λ decay in heavy hypernuclei) occurs between two successive beam bunches. An analyzing RF-resonator (RFR) is placed at the end of an isochronous-electron transport system as seen in Fig. 6, providing circular scanning of secondary electrons accelerated up to about 10 keV. The simulated time-of-flight of the secondary electron swarm from the target to the RF system is of the order of a few ns and a few ps in width [24,25]. The RF deflecting system consists of two resonant cavities, where the fields are perpendicular to each other and to the velocity of the electron swarm. Power with the same frequency feeds the resonators from accelerator wave-guides by means of a coaxial line. Therefore the system is locked in phase with the beam bunches. Standard RF phase shifters will be used for adjusting the entire system. Absolute time calibration by this method within subpicosecond resolutions is possible [27].

A position sensitive detector will be located at about 10 cm after the RF system. Determining the position of the center of gravity of the electron swarm with an accuracy of 0.1 mm is achievable with picosecond resolution at TJNAF. All the secondary electrons from the incident beam, or from promptly produced secondary particles, pass the RF deflecting system in the same phase, are deflecting by the same angle and hit the same place on the detector. They will be used as reference for calibration. The delayed secondary electrons are deflected differently as a function of the relative phase of oscillations in the cavity. Each fission fragment passing through the target surface produces ~150 secondary electrons. The spatial size of the swarm at the end of transportation is about 1 mm. It is assumed that the center of gravity of the electron swarm can be determined with an accuracy of 0.1 mm, which results in a time measurement with 0.5 ps precision. Both fragments of delayed fission events will be detected in a similar way (Fig. 6).

Streak cameras, based on similar principles, are routine techniques to obtain picosecond time resolution of the radiation from sources [28,29]. However, these techniques, although capable of very high time resolution, have a fairly short dynamic range. It is worthwhile to mention that the theoretical limit for this technique is about 10 fs [28].

4.3 The Neutron Detectors Based on Low-Pressure MWPC's

For the detection of neutrons in the 1-10 MeV energy range we propose to use neutron detectors consisting of foils of U-235 (~6 mg/cm^2 thickness) and low-pressure MWPCs (Fig.7). The neutrons will interact with uranium foil and cause fission. Fission fragments will be detected in low-pressure MWPCs. The properties of low-pressure MWPCs [30,31] are very suitable for this goal. Among the qualities are the following:

1. High rate capability;

2. Extreme insensitivity to gamma and relativistic particle backgrounds;

3. Good timing resolution (~200 ps, FWHM);

4. Good position resolution (~200 μm, FWHM);

5. High efficiency (~100%) for detecting fission fragments;

6. Negligible radiation damage;

7. No limitation on the size and shape.

Recently, we have developed low-pressure MWPCs for a time-zero fission fragment detector [31]. As desired by experiment E99-003 [32], timing and position resolution of about 200 ps (FWHM) and 800 μm (FWHM) for a chamber size of 21×21 cm^2 was achieved (Fig. 8). It was shown that Heptane, Hexane, and Isobutane gases at a pressure 1-3 Torr are all suitable for such a FF detector. The influence of the high radiation on the operation of the FF detector was tested by putting the detector near a beam at 7°, 20 m down from a 4% radiator +15 cm liquid deuterium target. We didn't notice any change in time resolution of the detectors up to 10 μA electron beam, which produces 10^9 electrons/second in the solid angle of the chamber according to Monte Carlo simulation [10]. At higher intensities (~50-70 μA) the signals decreased 2-3 times due to space charge effects, but the time resolution of FF from a Cf-252 source became worse by only 30%. The neutron detectors will cover angles above 20° to minimize the influence of the radiation on the chamber operation. We will use an Al absorber between the RF timing equipment and neutron detectors, not allowing low (<10 MeV) energy electrons to enter into low-pressure MWPCs. According to Monte Carlo simulation, 100 μA electron beam on a 2 mg/cm^2 Pb target will produce ~10^9 Moller electrons/second with energies higher than 10 MeV and scattering angles ranging from 20° to 180°. Therefore, for a 2 mg/cm^2 target we will have 200 ps (FWHM) time resolution of FF for an electron beam up to 100 μA. However, we have developed low noise amplifiers and can operate MWPCs at low gas gain, providing good resolution even in a twice higher radiation environment. The neutron ^{235}U fission cross section in the energy range 1-10 MeV is about 10^{-24} cm^2, and such a detector, for example, consisting of 10 layers uranium + MWPCs will have efficiency of the order of 10^{-4}. We can use foils from ^{238}U or from ^{10}B as a neutron converter. In the first case we will have low efficiency for ~1 MeV and low energy neutrons, in the second case about two times worse timing resolution due to detection of alpha particles instead of FF.

4.4 Resolutions

The expected intrinsic resolution of the RF timing technique is about $\sigma \approx 1$ ps. The width of the microbunch at CEBAF is 1.67 ps. The level of prompt fission events at $t=t_0$ from the center of microbunch is $\exp[-t_0^2/(2\sigma^2)]$ and is negligible already at t_0 =20 ps. The expected ratio of delayed to prompt fission events is about 10^{-4}, and about 90% of delayed fission events associated with the heavy hypernuclei (mean lifetime is ~200 ps) will be detected unambiguously in the time range greater than 20 ps.

Absolute calibration of the RF timing technique within 1 ps or better precision is possible, and the lifetime of the delayed fission events will be determined with a precision better than 1 ps.

The position and timing information provided by FF detectors allow reconstruction of the neutron time-of-flight with 200 ps (FWHM) precision. In Fig. 9 the energy resolution of neutrons for 10 cm flight distance is shown as a function of neutron energy. For 1 MeV neutrons we have better than 50 keV precision. A Monte Carlo simulation of the expected experimental energy spectra of 10^4 Auger neutrons for 20 cm flight distance, theoretical spectra of which are shown in Fig. 3[a,b], are presented in Fig. 10[a,b].

The absolute time and position calibration of the neutron detectors is assumed to be possible within 10 ps and 100 μm respectively. As a result the absolute value of the 1d-1s transition energy of Λ-states will be determined within a few keV precision.

4.5 Position sensitive detector for secondary electrons

The detector must be able to operate near the beam and provide a center of gravity for about 150 secondary electrons produced by delayed fission fragments and accelerated up to 10 keV, with a precision of 100 μm.

We plan to use two kinds of position sensitive detectors for secondary electrons. We suggest the use of a scintillation foil with a thickness of the order of 10 μm, with fiber optics and position sensitive PMTs [33]. We plan to carry out R&D to demonstrate the ability of such a simple system to provide, the necessary resolution and operate near the target.

We plan to carry out a study using low-pressure MWPC as a secondary electron detector. This technique is able to operate near the target, to separate fission events, and to provide the necessary resolution. But in this case we must solve a technical problem connected to the separation of the low-pressure gas volume (1-3 Torr) from the vacuum volume of RF timing equipment (10^{-3} Torr) by using thin foils, transparent for 10 keV electrons.

4.6 Short Orbit Spectrometer-SOS

The Short Orbit Spectrometer in Hall C will be used for the detection of K^+ mesons in coincidence with the RF timing technique to check the correlation of delayed fission events with heavy hypernuclei.

5. Rate and Background Estimates

Each delayed fission of heavy hypernuclei will produce 1-2 monochromatic, and 2-3 nonmonochromatic neutrons due to nuclear Auger, nonmesonic weak decay and fission processes.

From the condition:

$R_{Acc} \leq R_{Auger}$,

where R_{Acc} and R_{Auger} are the accidental and Auger neutron rates respectively, one can estimate the maximum accepted luminosity (or background neutron rate- N_n). For 10 ns time gate we have:

$\varepsilon \times N_n \times 10^{-8} \leq \varepsilon$

where ε is the neutron detection efficiency ($\varepsilon \approx 10^{-4}$) and for the maximum rate of background neutrons we have:

$N_n \leq 10^8$/s.

From the MC simulation for 1.6 GeV electrons and a lead target, for the cross section of the production of neutrons with energies lower than 10 MeV we have:

$\sigma(e+Pb \rightarrow n+X) \approx 30$ mb.

For a 2mg/cm^2 target the maximum intensity of incident electron beam is:

$N_e \approx 6 \cdot 10^{14}$ e/s.

The expected Auger to background neutron rate is:

$N_{Auger}/N_n = 10^{-5}$,

and for the neutron detectors with 10^{-4} efficiency the maximum Auger neutron rate is:

$N_{Auger} \approx 0.1$/s.

We are planning to take 10^4 events for each of two different targets: ^{208}Pb and ^{238}U. The expected probabilities of $^{208}_{\Lambda}$Pb and $^{238}_{\Lambda}$U to fission after weak decay $\Lambda N \rightarrow NN$ takes place are about 5% and 100% respectively. To take 10^4 events for each nucleus we need 30 hours for ^{238}U and 600 hours for ^{208}Pb. In addition to 26 days of beam time, we estimate 4-5 days beam time for the empty target run and for the calibration of the RF timing technique and multichannel neutron detector. Therefore we estimate a total of 30 days of beam time.

6. Summary

Using the high intensity, low emittance 2 GeV and 10-100 μA electron beam in Hall C at TJNAF, the RF picosecond timing technique of fission fragments, and an array of neutron detectors based on low-pressure MWPCs, the precise spectroscopy of the Auger neutrons via heavy hypernuclei photoproduction appears possible. The major scientific contribution of such an experiment lies in the fact that the new RF picosecond timing technique for fission fragments can be employed at CEBAF, and the deeply bound shell structure of the heavy hypernuclei can be investigated with a precision better than 100 keV. The absolute value of the 1d$\rightarrow$1s Λ major shells transition energy will be determined with a few keV precision. The lifetime of heavy hypernuclei will be determined as a by-product with picosecond precision.

The RF picosecond timing technique will enable to tag up to 1000 heavy hypernuclei per second at CEBAF and can be used in combination with other existing at JLab experimental equipment, e.g. with the CLAS detector, for detailed study of the four-baryon weak interaction.

References

1. L.S. Cardman, Nucl. Phys. A654 (1999)73c
2. B. Frois et al., Nucl. Phys. A396 (1983) 409
3. E. N. M. Quint et al., Phys. Rev. Lett. 57 (1986); and Phys. Rev. Lett. 58 (1987) 1088
4. H. Bondo, T. Motoba, Y. Yamamoto, Phys. Rev. C31(1985) 265
5. R. E. Chrien, in Proc. LAMPF workshop (π, K) Physics, Los Alamos, NM 1990; eds B. F. Gibson, W. R. Gibs, M. B. Johnson, AIP (New York 1991) p. 28
6. A. Likar, M. Rosina, B. Povh, Z. Phys. A324 (1986) 35
7. E. Hungerford, R. Chrien, L. Tang (co-spokespersons) TJNAF E-89-009, Investigation of the ΛN Effective Interaction in the P Shell.
8. Shian S. Hsiao and Stephen R. Cotanch, Phys. Rev. C28, n4 (1983) 1668
9. J. Berthot, P. Y. Bertin, (γ, K_s^0): an alternative to (γ, K^+) for hypernuclei studies? Research program at CEBAF(III), Report of the 1987 Summer Study Group, 1987, p.406
10. P. Degtyarenko, Experimental proposal for the determination of neutron spectra from targeted electron beam, JLAB-ACC-96,1996
11. A. Margaryan, G. Oksuzyan, Proposal for RF timing of delayed fragments and recoil nuclei in the picosecond range, Preprint YERPHI-1489(6)-97 (1997)
12. A. Margaryan, Picosecond Timer, ISTC Project A-372 (1999)
13. L. E. Tzopp, Radio Engineering and Electron Physics 4,1936 (1959)
14. V. P. Bykov, Soviet Physics JETP 13, n6, 1169 (1961)
15. X. J. Wang, X. Qiu, and I. Ben-Zvi, Phys. Rev. E 54, R3121 (1996)
16. B. Johanson and T. Alvager, Nucl. Instr. And. Meth. 3, 49 (1958)
17. A. E. Blougrrund, Y. Dar, and G. Goldring, Phys. Rev. 120, 1328 (1960)
18. G. Goldring, Nucl. Instr. And Meth. 11, 29 (1961)
19. A. E. Blougrund et al., Nucl. Phys. 45, 54 (1963)
20. A. E. Blougrund et al., Nucl. Phys. 69, 423 (1963)
21. I. Ben-Zvi et al., Nucl. Phys. A117, 625 (1968)
22. I. Ben-Zvi et al., Nucl. Phys. A135, 153 (1969)
23. E. W. Ernst and H. von Foerster, J. Appl. Phys. 26, 781 (1955)

24. A. M. Zibelman et al., Nucl. Instr. And Meth., 141, 439 (1977)

25. J. D. Bowman and R. H. Heffner, Nucl. Instr. And Meth., 148, 503 (1978)

26. R. L. Kavalov et al., Nucl. Instr. And Meth. A237, 543 (1985)

27. Alex Lumpkin, Time-Domain Diagnostics in the Picosecond Regime, AIP Conference Proceedings 367, 1995, p.327

28. E. K. Zavoiski and S. D. Fanchenko, Appl. Optics, V.4, n. 9, 1155 (1965)

29. M. M. Murname et al., Appl. Phys. Lett. 56, 1948 (1990)

30. A. Breskin, G. Charpak, S. Majewski, Nucl. Instr. and Meth. 220 (1984) 349

31. K. Assamagan et al., Nucl. Instr. and Meth. A426 (1999) 405

32. L. Tang, A. Margaryan (Co-spokespersons), TJNAF (E-95-002) E-99-003, Direct Measurement of the Lifetime of Heavy Hypernuclei at CEBAF.

33. G. Comby and R. Meunier, Nucl. Instr. And Meth., A269, 246 (1988)

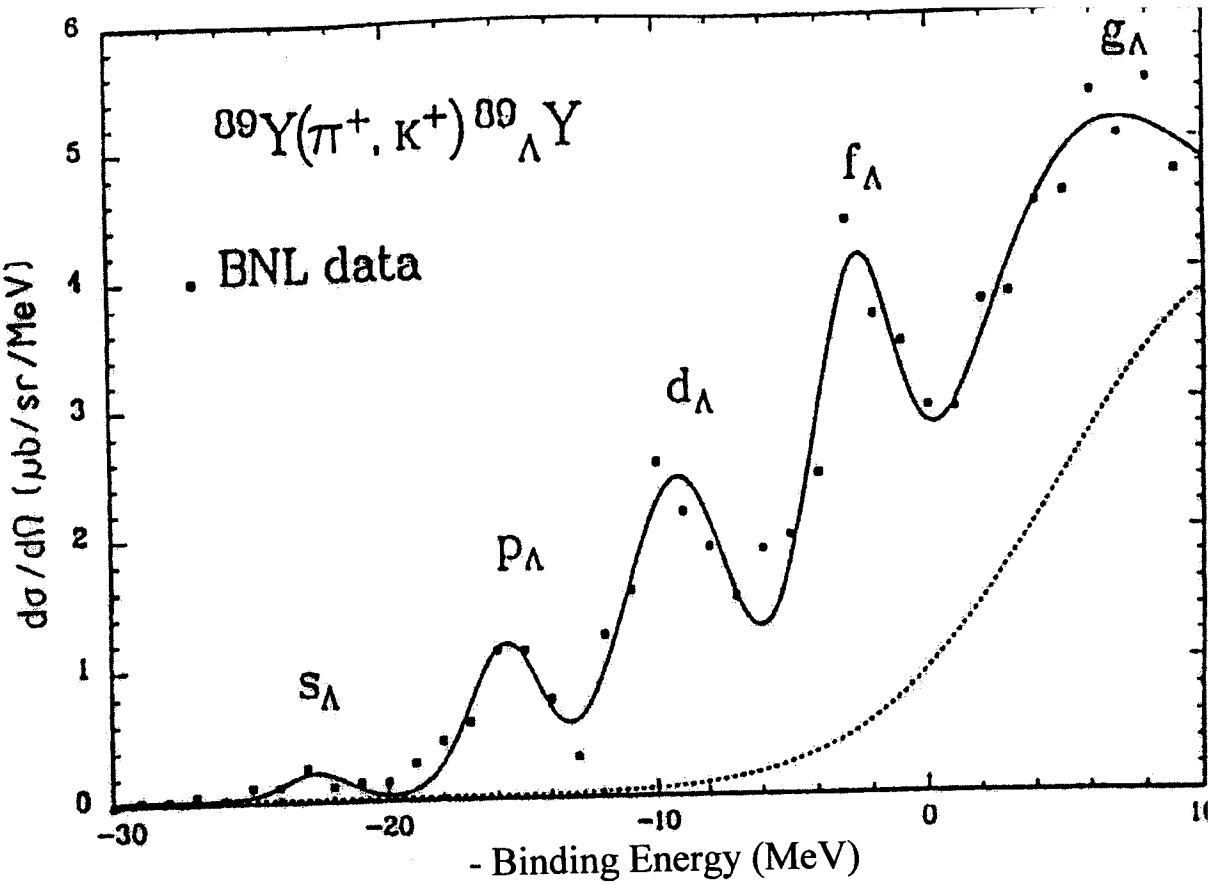

Fig. 1 Hypernuclear states obtained in the $^{89}Y(\pi^+,K^+)^{89}_{\Lambda}Y$ reaction, showing the Λ in the s, p, d, f and g orbits, as measured at AGS. The solid line represents a DWBA calculation (from Ref. [5]).

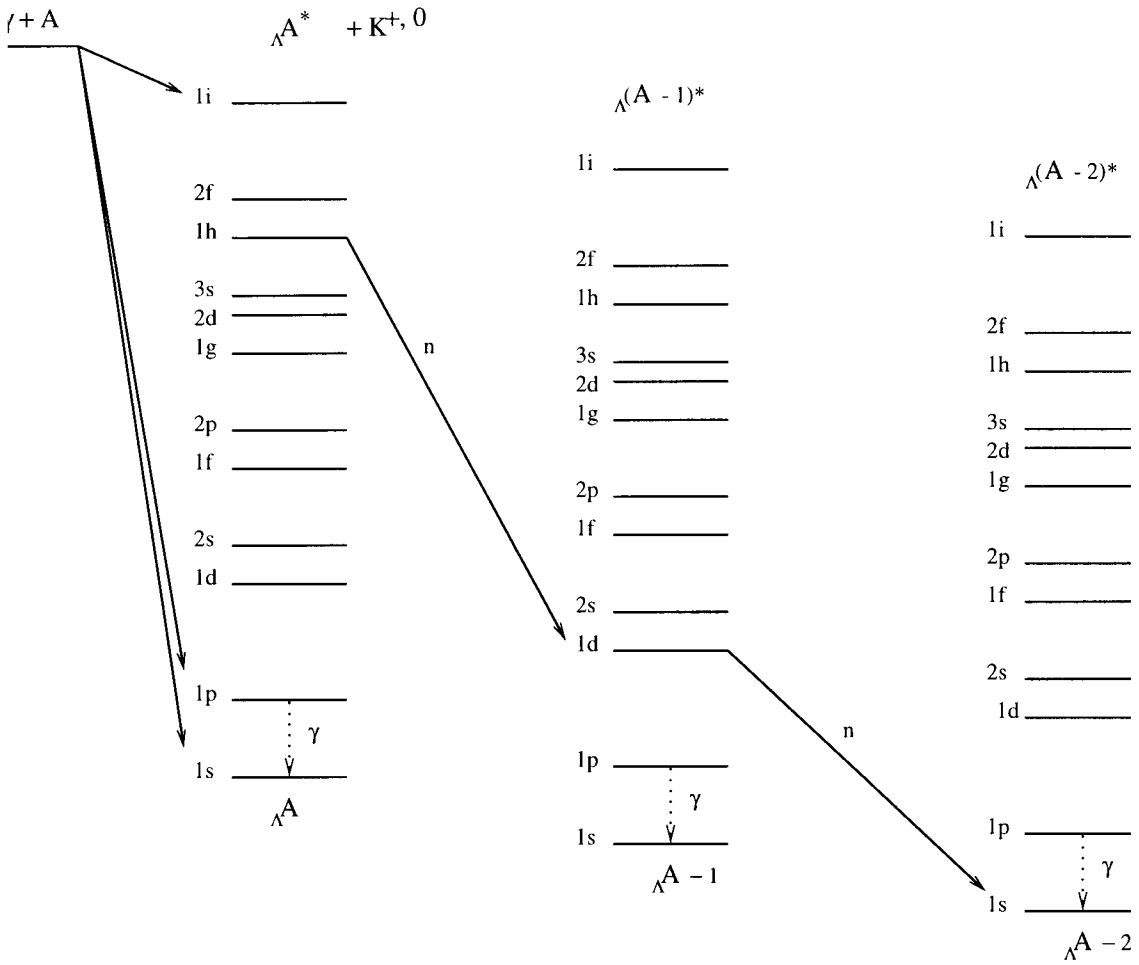

Fig.2 Schematic representation of the photoproduction of a heavy excited hypernuleus and Auger neutron emission processes.

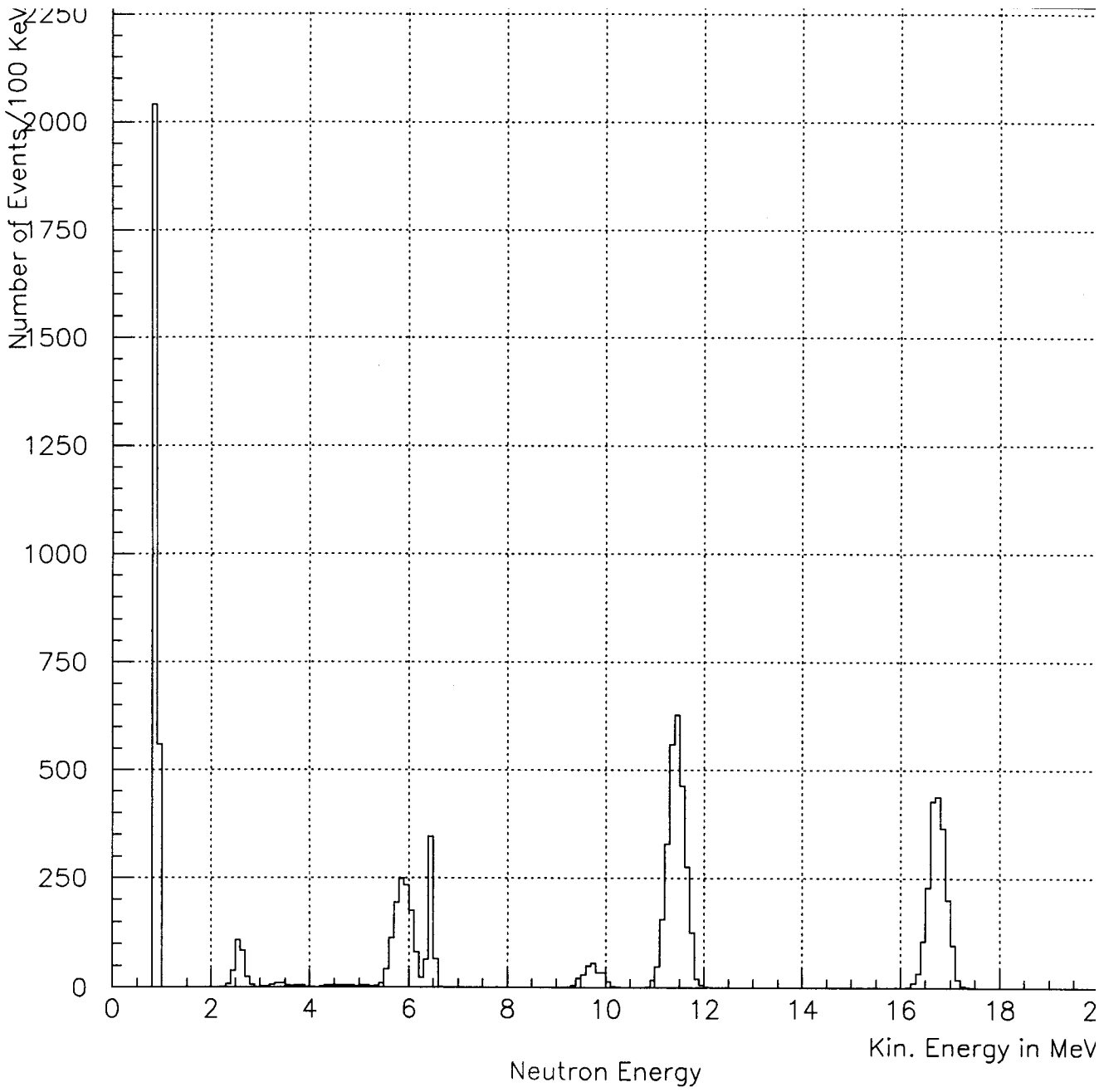

Fig. 3[a] Theoretical energy spectrum of the Auger neutrons after the deexcitation of 1h state of $^{208}_{\Lambda}$Pb for the "A" choice of Λ potential.

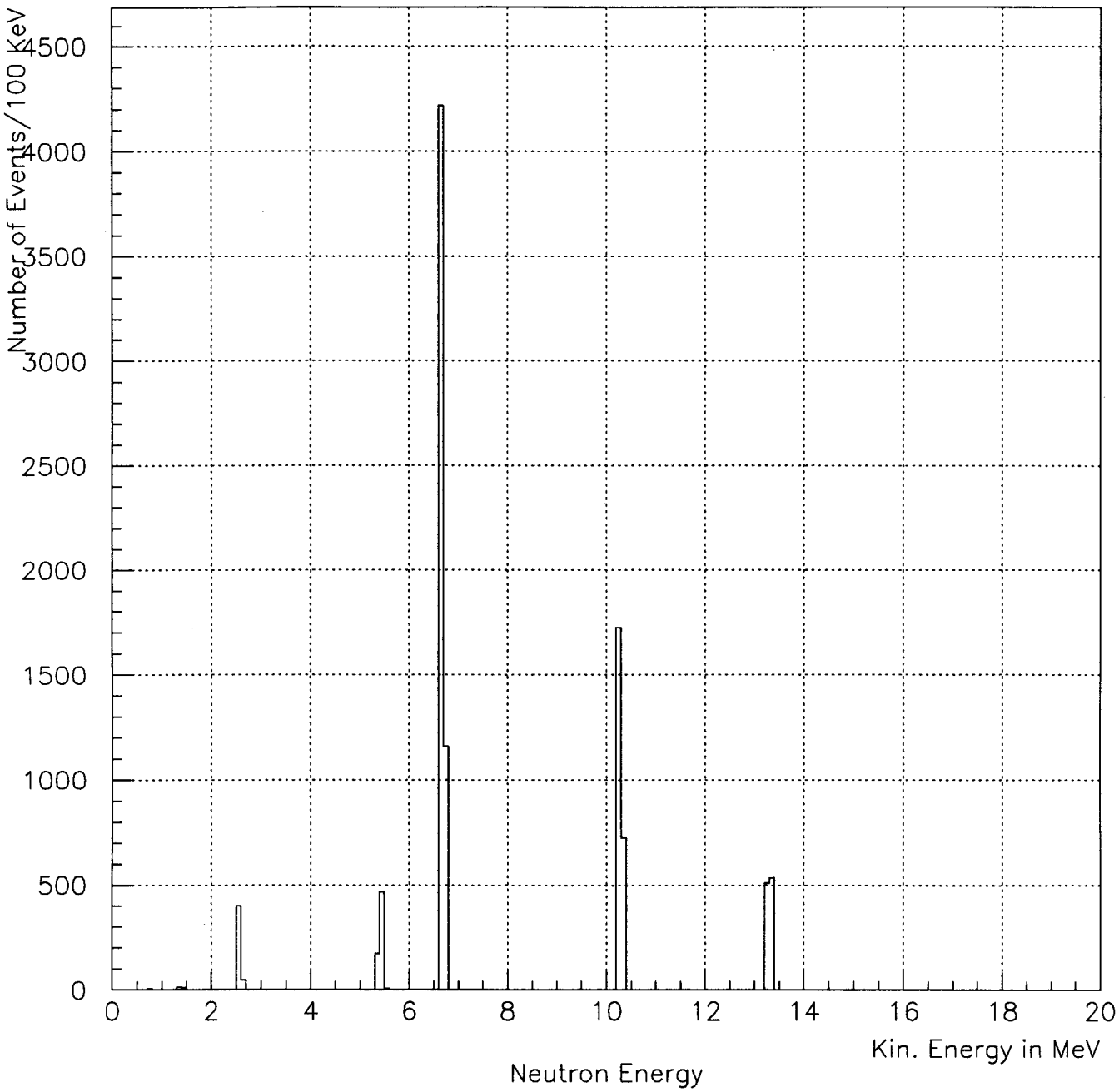

Fig. 3[b] Theoretical energy spectrum of the Auger neutrons after the deexcitation of 1h state of $^{208}_{\Lambda}Pb$ for the "B" choice of Λ potential.

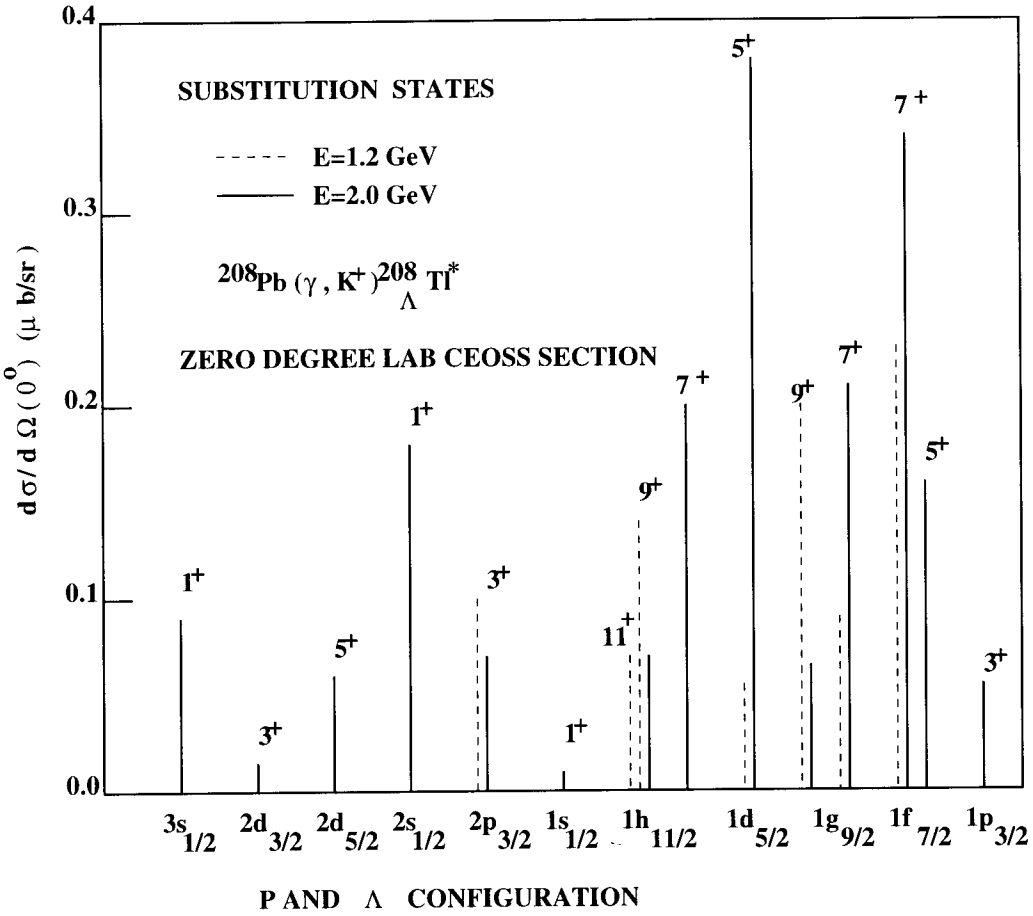

Fig. 4 Dominant substitution states predicted for $^{208}_{\Lambda}$Tl. For each Λ and p single particle configuration (identical) the largest cross section and corresponding final spin parity is represented. In this figure, cross sections are plotted for E=1.2 GeV (dashed lines) and 2.0 GeV (solid lines), from ref. [8].

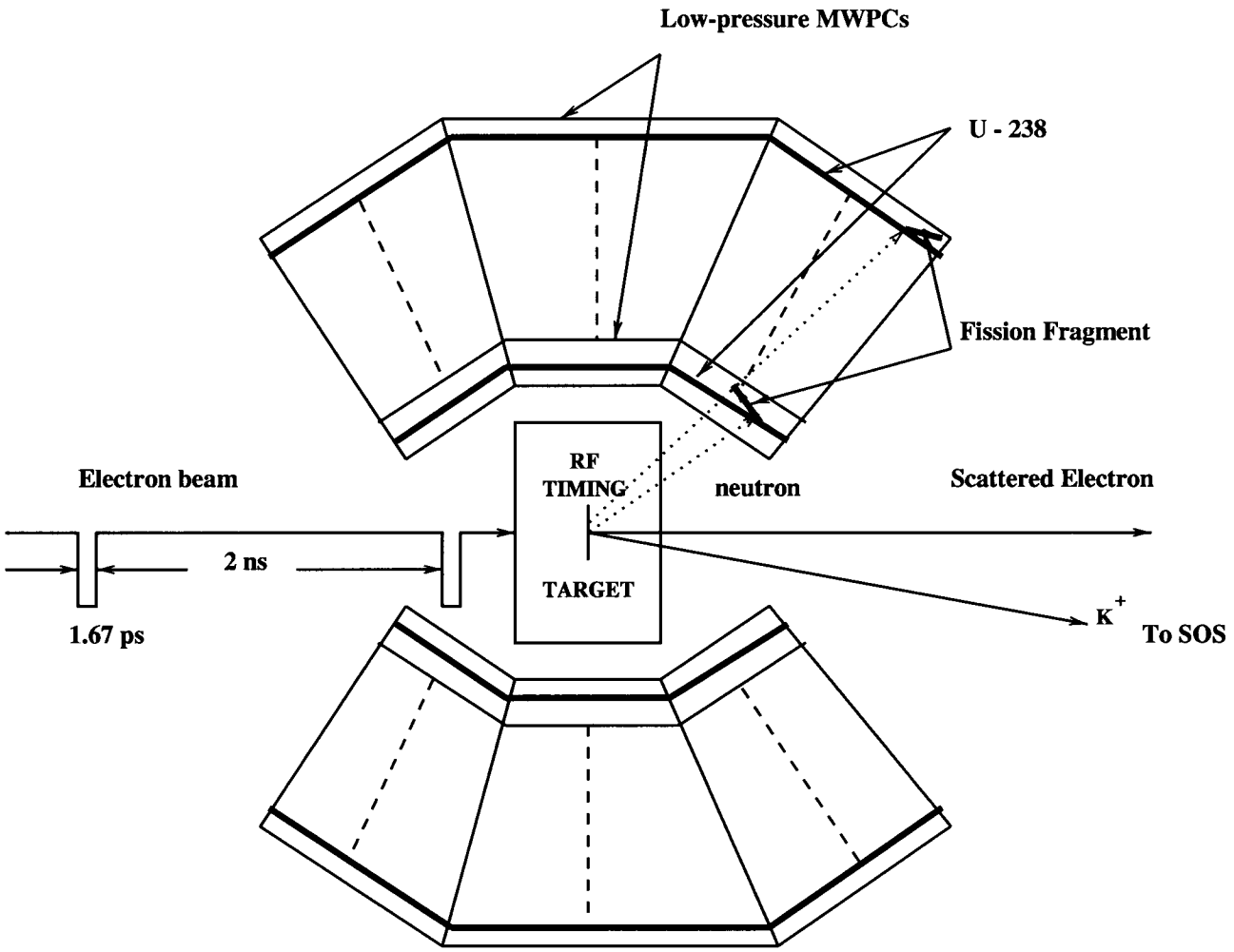

Fig.5 A schematic representation of the experimental setup for Auger neutron specroscopy

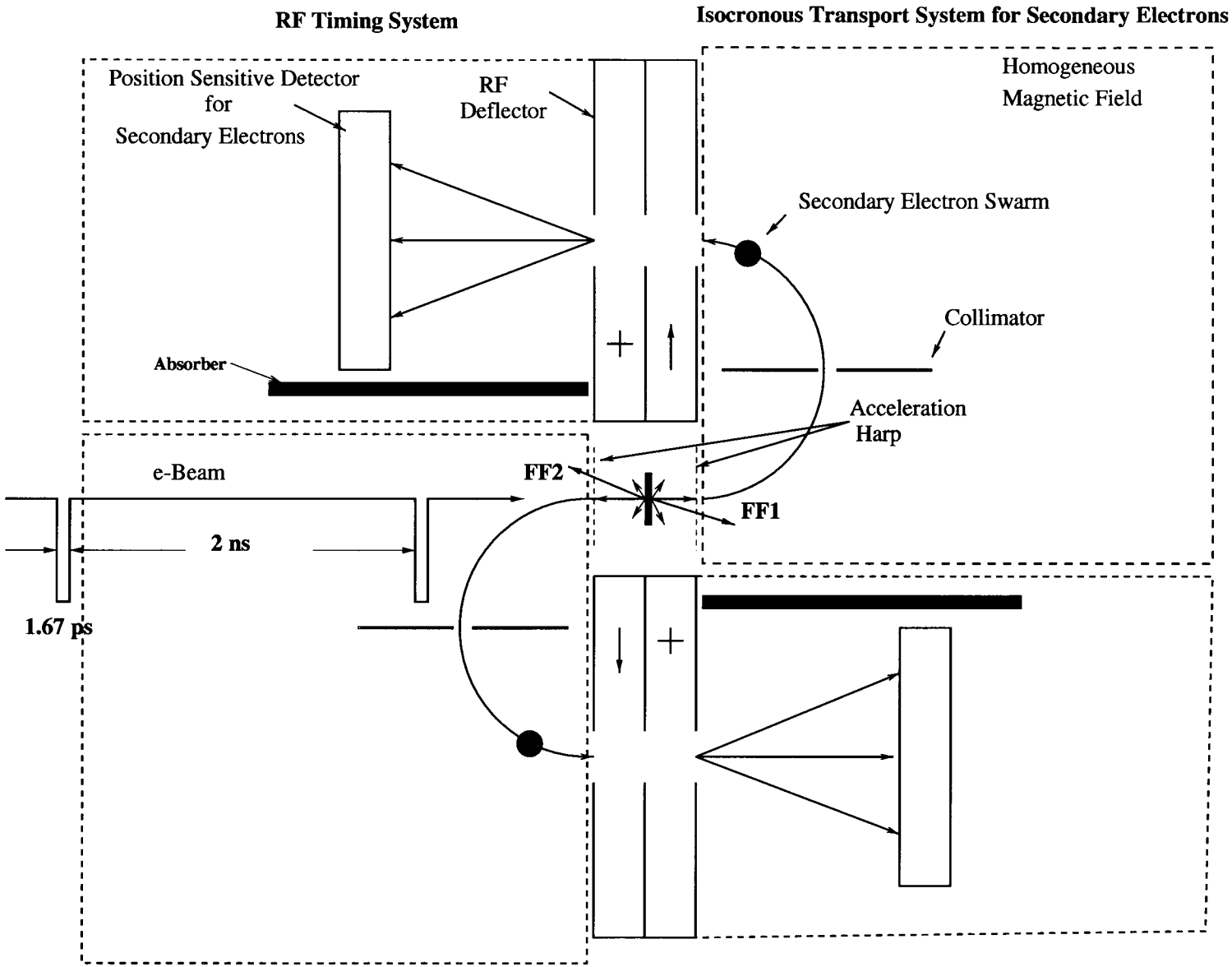

Fig.6 The principal scheme of the RF timing technique. + - field pointed into the page.

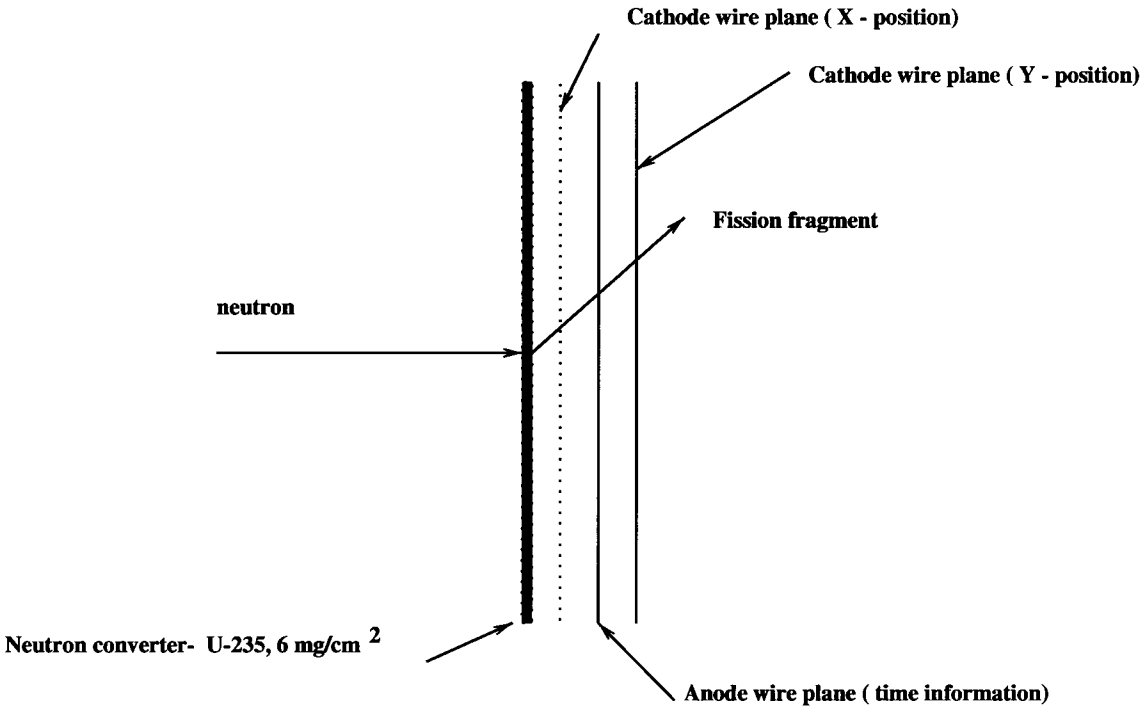

Fig. 7 Schematic scetch of the neutron detector

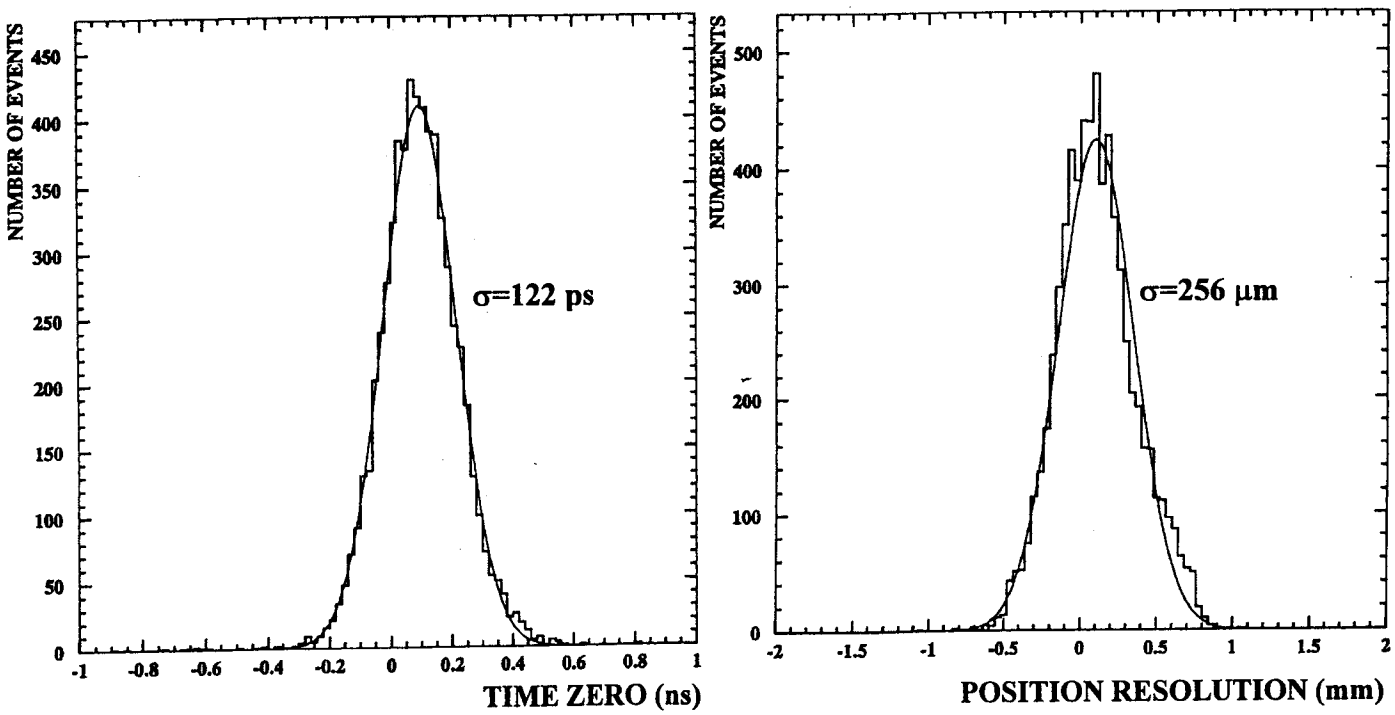

Fig. 8 Time-zero and position distribution of fission fragnents from ^{252}Cf source. Heptane 1.3 Torr.

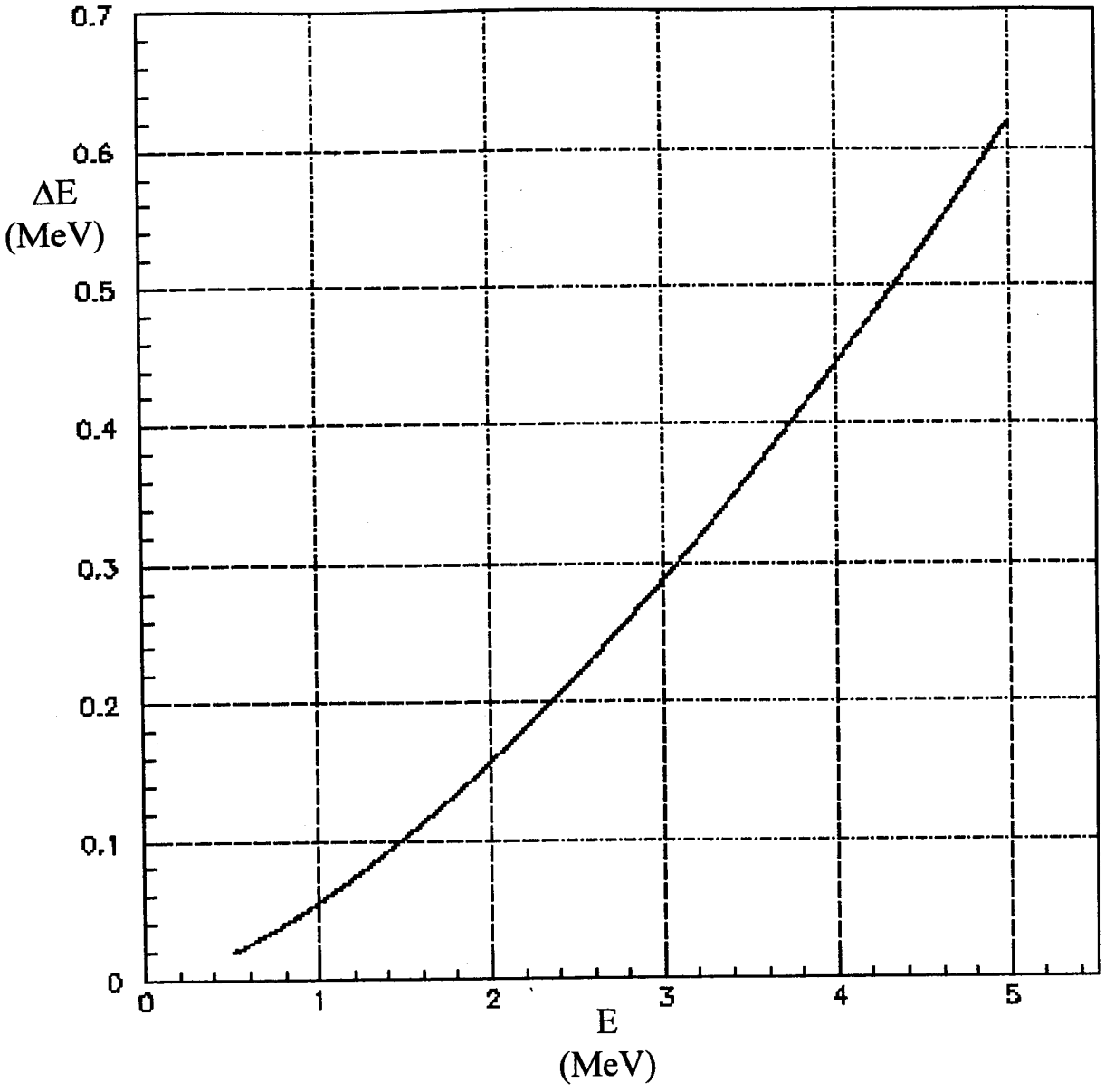

Fig. 9 Energy resolution (FWHM) of time-of-flight neutron spectrometer. Flight distance 10 cm, time resolution 200 ps (FWHM).

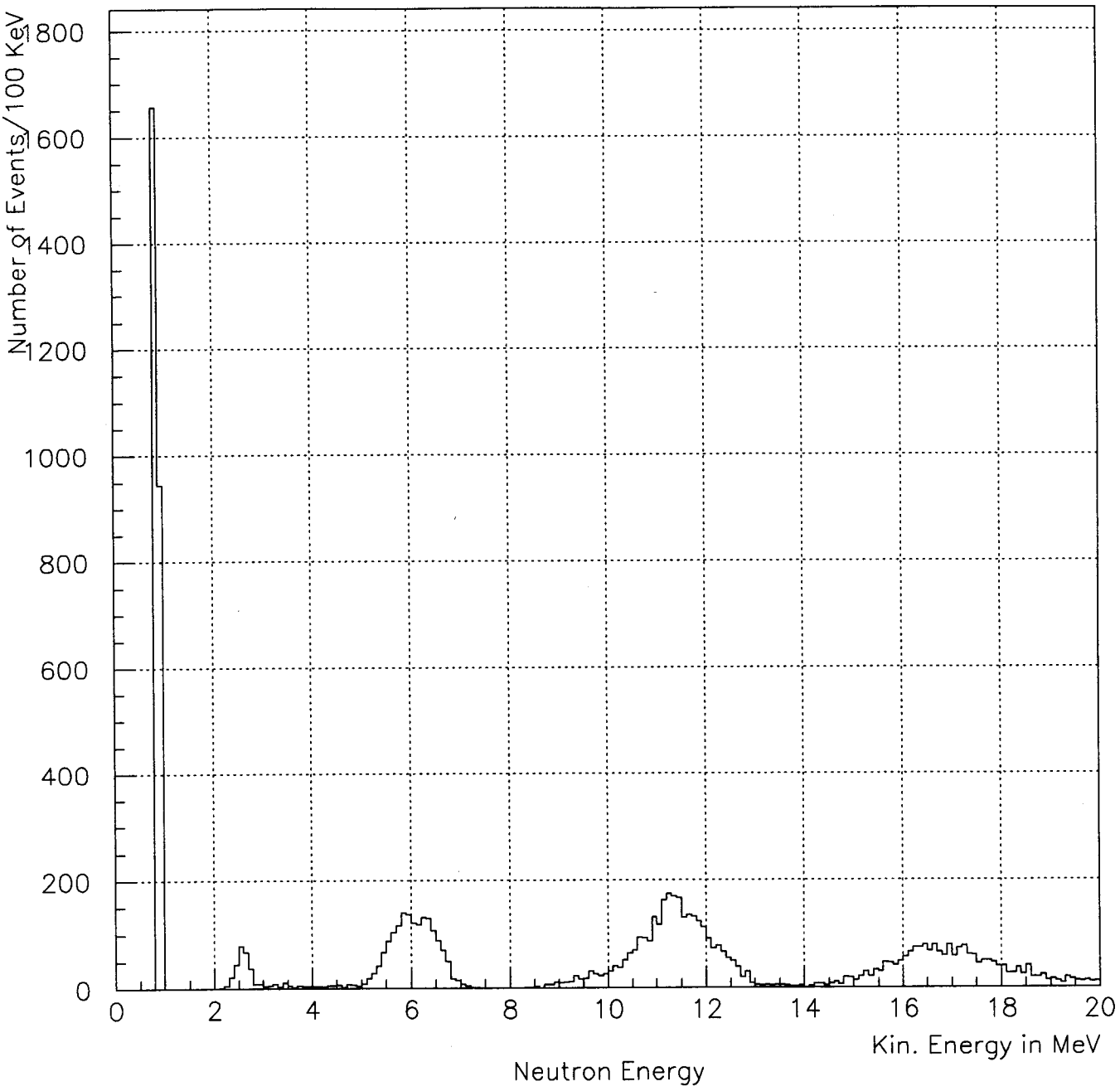

Fig. 10[a] Expected experimental energy spectrum of the Auger neutrons after the deexcitation of 1h state of $^{208}_{\Lambda}$Pb for the "A" choice of Λ potential.

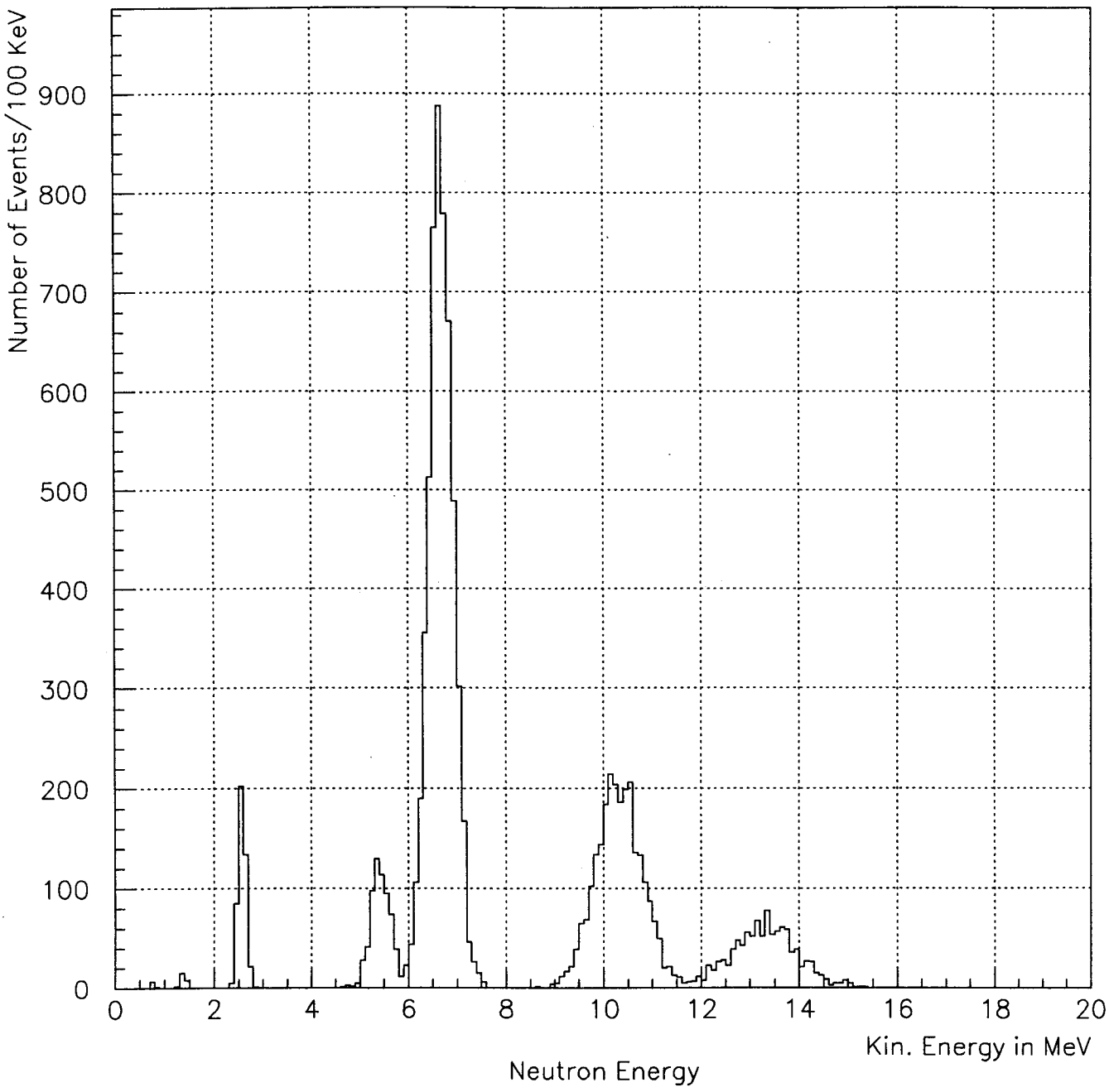

Fig. 10[b] Expected experimental energy spectrum of the Auger neutrons after the deexcitation of 1h state of $^{208}_{\Lambda}$Pb for the "B" choice ofΛ potential.